Ion implantation into gallium arsenide

R. Anholt,[a] P. Balasingam, S. Y. Chou, and T. W. Sigmon
Solid State Electronics Laboratory, Stanford University, Stanford, California 94305

M. Deal
Center for Integrated Systems, Stanford University, Stanford, California 94305

(Received 18 March 1988; accepted for publication 8 June 1988)

Secondary-ion-mass-spectrometry studies of the implantation profiles of 20- to 400-keV Si, Se, and Be ions into GaAs are reported. The measured profiles are fit with Pearson-IV distributions whose moments are fit to functions of the ion energy to obtain simple, widely applicable analytical formulas. Also, profiles are measured for varying wafer tilt and rotation angles to the ion beam, and for varying dislocation densities and doses. For implantation through dielectric caps, the profiles in the GaAs can be simulated using shifted, bare-wafer Pearson-IV distributions for Be, or mixtures of shifted Pearson-IV and Gaussians for Si and Se. Also, knock-on distributions of Si and O atoms resulting from implanting through SiO_2 caps were measured.

I. INTRODUCTION

For ion implantation into crystalline materials, the wafers must be tilted and rotated precisely with respect to the beam to minimize axial and planar channeling.[1-8] This, however, will never completely eliminate channeling effects, since the ions undergo hundreds of collisions before they come to rest, and they have a finite probability of scattering into a channel during any single collision. In a channel, the ion stopping power is reduced, resulting in a fraction of the ions coming to rest at depths much deeper than would occur in an amorphous material. This partial channeling is responsible for exponential tails observed in implanted atomic-impurity profiles in crystalline materials.

Several methods are available to calculate profiles of ions implanted into amorphous materials.[9-13] Figure 1 compares a measured profile for 80-keV Si ions implanted into GaAs with a profile calculated using the TRIM Monte-Carlo code[10] for an identical implant into amorphous GaAs. Similar results are obtained when comparing with other implant calculations[9,11,12]; the amorphous codes predict a narrower distribution and fail to predict the exponentially falling channeling tails.

The aim of the present work is to develop the best possible simulations for ion implantation profiles in GaAs, for use in process and device-modeling codes being developed for GaAs digital and monolithic-microwave integrated-circuit technology. GaAs metal-semiconductor field-effect transistor (MESFET) device characteristics depend critically on the threshold voltage V_{th}, which in turn depends on the pinch-off voltage V_p given by[14]

$$V_p \simeq V_{bi} - V_{th},$$

$$V_p \sim \frac{q}{\epsilon_0 \epsilon_r} \int_0^\infty x\, dx\, N_D(x), \quad (1)$$

where V_{bi} ($\sim$0.8 V) is the barrier height of the Schottky gate junction. The pinch-off voltage is directly proportional to the first moment of the implanted donor concentration distribution $N_D(x)$. As a result of channeling, a fraction of the ions are implanted at deeper depths, resulting in higher moments, higher pinch-off voltages, and more negative threshold voltages than calculated for equal-dose implants into amorphous material. Since quantities like the drain-source current at zero gate voltage depend upon the square of the threshold voltage, it is vital to correctly model implant profiles into crystalline GaAs to be able to correctly predict device characteristics.

The method we have adopted to simulate ion-implantation profiles in GaAs, is to fit analytical distributions to measured profiles. The advantage of this method is that numerical profiles can be calculated rapidly, as opposed to Monte-Carlo or Boltzmann-transport calculations.[10,11] Also, Monte-Carlo and Boltzmann-transport codes incorporating crystalline structures have not been sufficiently developed to be widely available.[15-19] The disadvantage of our approach is that one can never fully explore all implant profiles of conceivable use. In this work, we only study profiles of Be, Si, and Se ions in GaAs. These ions were chosen be-

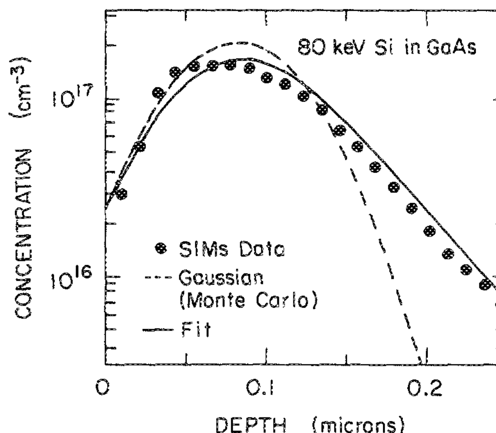

FIG. 1. Comparison of a measured 80-keV Si^{29} implant concentration profile with a profile calculated using the TRIM Monte-Carlo code,[10] and with a fit.

[a] Present address: Gateway Modeling, 1604 East River Terrace, Minneapolis, MN 55414.

 0021-8979/88/193429-10$02.40 © 1988 American Institute of Physics

Downloaded 08 Aug 2003 to 128.112.49.65. Redistribution subject to AIP license or copyright, see http://ojps.aip.org/japo/japcr.jsp

cause Si and Se are the most widely used donor impurities in GaAs MESFET technology, and Be is used to produce buried acceptor layers in MESFETs. Furthermore, these three ions encompass a wide range of possible atomic numbers, so that eventually it may be possible to interpolate parameters for calculating the profiles of intermediate atomic numbers using data from these three.

In Sec. II of this paper, we describe our secondary-ion-mass-spectrometry (SIMS) measurements. In Sec. III, results of profile studies are described for (a) the ion-energy dependence in bare, uncapped GaAs wafers, (b) the wafer tilt and rotation dependence, (c) the dependence on the ion dose, and (d) the dependence on the wafer dislocation density. In Sec. III E, methods are formulated for calculating the profiles of ions implanted through SiO_2 or Si_3N_4 caps, and in Sec. III F, measurements of the profiles for "knock-on" Si and O atoms, resulting from implantation through SiO_2 caps are discussed. Section III G comments on the relationship between SIMS measurements of donor profiles and electron carrier profiles in liquid-encapsulated-Czochralski (LEC) grown GaAs. Finally, Sec. IV contains the conclusions.

II. MEASUREMENTS

Samples of commercial, high-pressure, LEC-grown, $\langle 100\rangle$-oriented GaAs wafers were implanted with Be^9, Si^{29}, and Se^{80} ions at doses of approximately 10^{13} cm^{-2} (except where noted). SIMS measurements of the as-implanted profiles were made at Charles Evans and Associates. This ion dose was chosen to obtain adequate SIMS statistics for modeling. Unless specified, the wafer tilt and rotation angles were 7° and 9° from the wafer major flat, respectively. The samples were cleaved parallel to the major $(01\bar{1})$ flat, and were bonded to Si wafers at the desired rotation for implantation, or were implanted using a goniometer to position the samples.

For each measured SIMS profile, a constant background concentration, obtained by averaging the concentrations in the deep, flat portions of the spectra, was subtracted. Also, SIMS measurements often give high surface concentrations, due to contaminants or varying sputter rates, that are unrelated to the actual implant profile. We replaced these concentrations, C_i, by values obtained by extrapolating the first few realistic points in each spectrum to shallower depths. Using these corrected profiles, we then calculated the moments of the distribution $\langle x^n\rangle$ using

$$\langle x^n\rangle = \sum_i x_i^n C_i \Big/ \sum_i C_i. \qquad (2)$$

For Pearson-type distributions, the normalized moments are defined as[20-22]

$$R_p = \langle x^1\rangle,$$
$$\Delta R_p = \sqrt{\langle x^2\rangle - \langle x\rangle^2},$$
$$\gamma = \langle x - R_p\rangle^3/\Delta R_p^3,$$

and

$$\beta = \langle x - R_p\rangle^4/\Delta R_p^4, \qquad (3)$$

where the first moment R_p is referred to as the projected range, and is the position of the peak of the distribution for Gaussian distributions. ΔR_p is the width of the distribution, projected on the depth axis. The normalized third moment γ describes the skew of the distribution. Positive values of the order of unity and larger describe distributions falling off approximately exponentially at large depths, while negative values describe distributions skewed toward shallower depths. The kurtosis factor β mainly decides the type of mathematical function best describing the distribution, according to whether it falls between certain ranges that are functions of γ [see, e.g., Eq. (4) below].[20-22]

In this paper, we are mainly interested in the shapes of the distributions. In most of the data shown below, the profiles have been normalized to arbitrary peak heights; the absolute peak heights can be obtained by normalizing the integrated area to the implanted ion doses.

To reduce SIMS artifacts and uncertainties, we measured most atom distributions at least twice using two different SIMS setups. Also, some distributions were independently implanted at several different times using up to two different implanters. When differences were observed, different samples were measured two additional times using the same SIMS setup. These precautions were taken to increase our confidence that these data, especially for the energy dependence of the unencapsulated implants, are accurate, and are independent of either the SIMS measurement or the ion-implant apparatus.

III. RESULTS

A. Ion-energy dependence

Figures 2 and 3 show moments for the distributions of Be, Si, and Se ions implanted into GaAs as a function of the ion energy, while Figs. 4–6 compare the measured distributions with profiles calculated using Pearson-IV distribu-

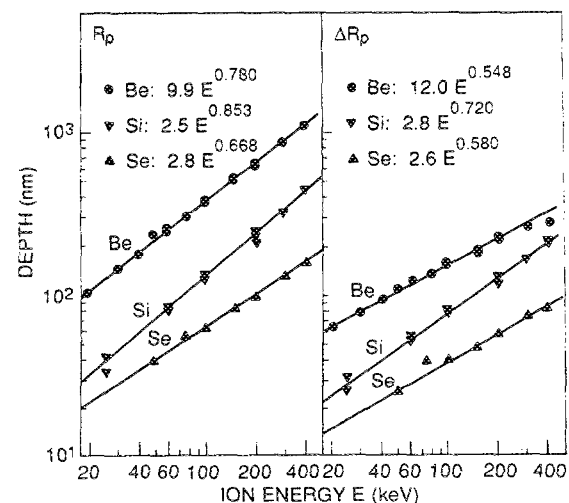

FIG. 2. Measured moments R_p and ΔR_p of concentration distributions of 20–400-keV Be, Si, and Se ions implanted into GaAs, and power-law fits (for ion energies in keV). The 10^{13} ions/cm^2 implants were done into bare wafers at a tilt and rotation angle of 7° and 9°, respectively.

Downloaded 08 Aug 2003 to 128.112.49.65. Redistribution subject to AIP license or copyright, see http://ojps.aip.org/japo/japcr.jsp

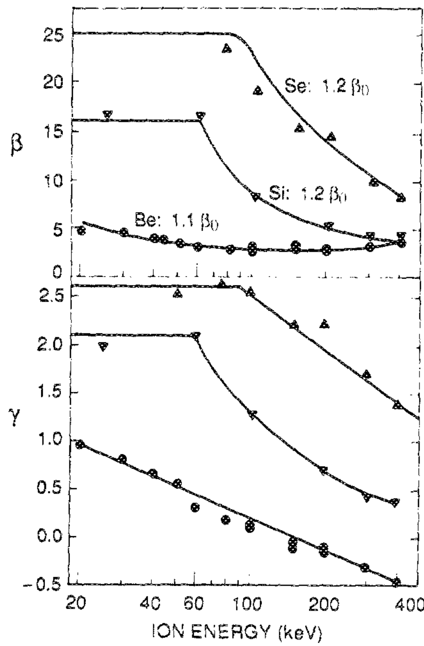

FIG. 3. Normalized third and fourth moments γ and β of concentration distributions of Be, Si, and Se ions implanted into GaAs, as in Fig. 2. β_0 is defined in Eq. (4). The γ values were fit to $\gamma = 2.38 - 1.1 \ln E$, for Be, $\gamma = \text{minimum}\ (2.1,\ 95E^{-0.93})$, for Si, and $\gamma = \text{minimum}\ (2.6,\ 6.2 - 1.8 \ln E)$, for Se, where E is the ion energy in keV.

tions. To use a Pearson-IV distribution for any set of moments, the value of the normalized fourth moment β must be greater than β_0, defined as[20–22]

$$\beta_0 = [39\gamma^2 + 48 + 6(\gamma^2+4)^{3/2}]/(32-\gamma^2). \qquad (4)$$

We usually find that the measured moments for the profiles automatically satisfy this criterion. Using Pearson-IV distributions to predict the profiles of ions implanted into crystals has the advantage of built-in exponential tails. An alternative way often used for fitting measured implant profiles is to add an exponential tail to a Gaussian distribution,[21] which is calculated using an amorphous implant code. Such distributions require the same number of fitting parameters, but the

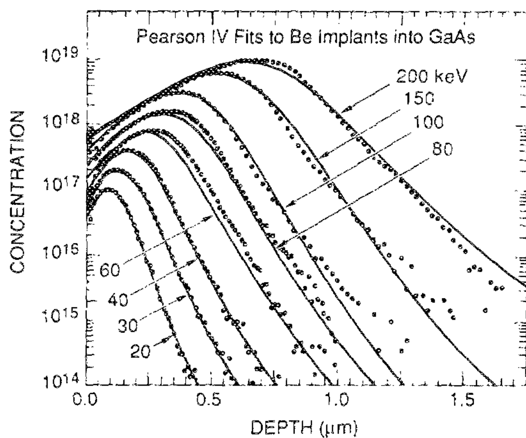

FIG. 4. SIMS measured profiles for 20–200-keV Be ions in GaAs, compared with Pearson-IV fits calculated with the parameters given in Figs. 2 and 3. The concentration distributions are normalized to arbitrary peak heights.

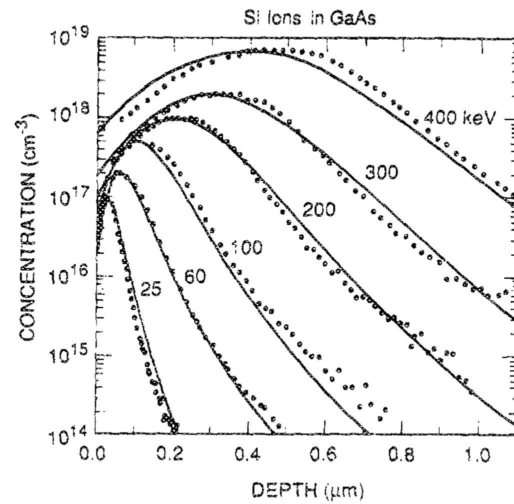

FIG. 5. SIMS measured profiles for 25–400-keV Si ions in GaAs, compared with Pearson-IV fits.

parameters are not as straightforwardly obtained from the distribution moments as they are for Pearson-IV distributions. On the other hand, the Pearson-IV distribution is more complicated to compute than a Gaussian, and can easily give computer overflow errors if not properly calculated.[23]

The moments R_p and ΔR_p shown in Figs. 2 and 3, were fit to power-law functions of the ion energy, γ was fit to either a linear function of log (E) or a power-law function of E, with a maximum, and β was fit to a constant multiplied by β_0. Due to statistical uncertainties, the third and fourth moments are less accurate than the first two; however, they also have less effect on the derived distributions. We have little data to support the use of a constant γ value for Si and Se ions below 100 keV; the present form was chosen for simplicity, instead of some more complicated parabolic function of log (E).

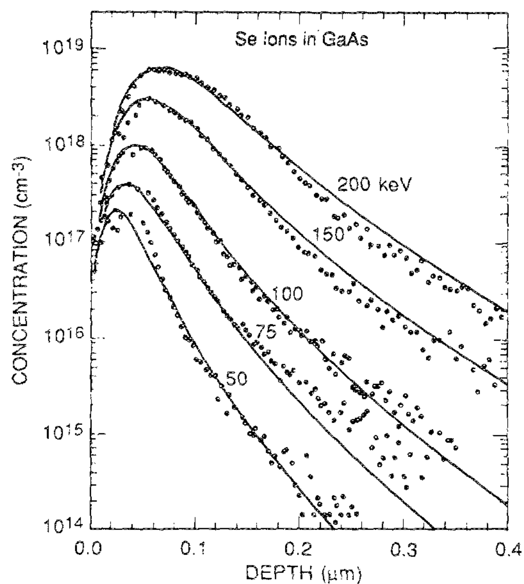

FIG. 6. SIMS measured profiles for 50–200-keV Se ions in GaAs, compared with Pearson-IV fits.

Downloaded 08 Aug 2003 to 128.112.49.65. Redistribution subject to AIP license or copyright, see http://ojps.aip.org/japo/japcr.jsp

Implanting Se ions for MESFET active channels instead of Si ions could be advantageous if, for the same R_p, the channeling tails of the Se profiles are significantly smaller than those for the Si ion profiles. Using the formulas in Fig. 2, and setting the R_p values for Si and Se ions equal, allows us to find the Se ion-energy E_{Se} needed to obtain the same R_p as Si ions with energy E_{Si}

$$E_{Se} = 0.829 E_{Si}^{1.28}. \quad (5)$$

This formula predicts, for example, that for a Si energy of 50 keV, the equivalent Se energy is 125 keV. In Fig. 7, we compare Pearson-IV fits to measured profiles for Si and Se ions. Also shown in Fig. 7, are calculated threshold voltages for Si and Se ions implanted to a dose of 2×10^{12} cm^{-2} at R_p matching energies and for an activation of 80%. For ion energies giving the same R_p values, nearly identical profiles and threshold voltages are obtained using Si and Se ions, despite the differences in the higher moments of the implant distributions. We therefore conclude that bare-wafer Si and Se ion profiles with energies related using Eq. (5) should give identical MESFET device characteristics if effects due to different activation, increased trap formation by the more highly damaging Se ions, and other factors are identical or negligible. If one chooses the Si and Se energies on the basis of the TRIM or LSS range tables,[9] different device characteristics may be obtained. Using matching R_p values from the LSS tables, one might choose a Se energy of 116 keV to compare with 50-keV Si ions. Since the Se ion energy is lower than required to match the measured profiles as in Fig. 7, such a comparison would give marginally higher transconductances for the Se ion-implanted devices, due to the slightly lower energy and resultant narrower profiles.

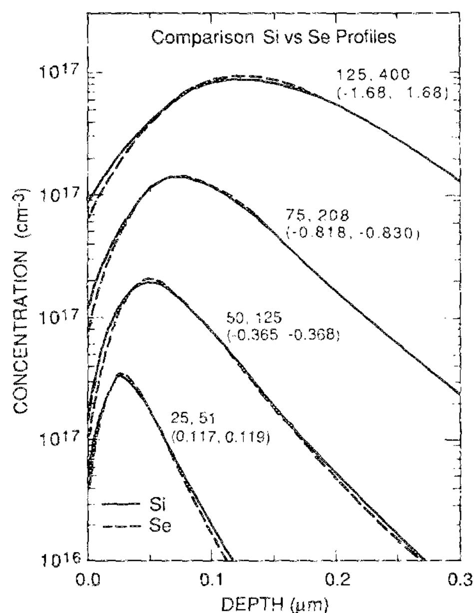

FIG. 7. Comparison of Si and Se profiles for energies selected to match R_p values calculated by Eq. (5). The ion energies in keV are shown beside each profile (the larger one being for Se). The numbers in parentheses are the corresponding threshold voltages calculated for the pair of profiles, assuming a constant dose and the same activation for both ions.

B. Tilt and rotation dependence

We investigated the effect of varying the wafer tilt and rotation angles θ_{tilt} and θ_{rot} to reduce the magnitudes of the channeling tails. Ziegler and Lever[3] have mapped the channel directions in Si (essentially the same lattice structure as GaAs) using He backscattering. As a function of the rotation angle, planar channeling should occur at 0°, 18°, and 45° from the ⟨001⟩ pole, and axial channeling should occur at various tilt angles for a rotation angle of 22°. The map suggests that the best rotation angle, with a standard tilt of about 7°, should be at about 9° or 36° from the major flat on $(01\bar{1})$ for SEMI-standard ⟨100⟩-oriented LEC GaAs. On the other hand, the widest planar channel is the (011). To avoid this channel, the impinging angle θ_{110}, given by[6]

$$\tan \theta_{110} = \tan \theta_{tilt} \sin \theta_{rot}, \quad (6)$$

should be greater than about twice the critical angle ψ_c, given by[6]

$$\psi_c(\text{planar}) \simeq 0.7\sqrt{2\pi Z_1 Z_2 e^2 N d_p a / E}, \quad (7)$$

where Z_1 and Z_2 are the projectile and target ($\simeq 32$ for GaAs) atomic numbers, N is the target-atom density, d_p is the distance between planes, and a is the Firsov screening length. For 60-keV Si ions, $2\psi_c$ is equal to $\sim 7°$. For these ions θ_{110} is less than twice the critical angle for every tilt angle less than 10° and every rotation angle, suggesting that avoiding planar channeling is impossible for this implant.

However, the magnitude of the channeling tails possibly can be reduced by keeping the tilt and rotation angles as large as possible. Several authors have suggested using tilt angles of at least 7° and rotation angles of 45° for implantation into Si and GaAs.[1,2,5,6] Even if θ_{110} is larger than $2\psi_c$, this will not completely avoid channeling, since partial channeling results from the multiple collisions the ion undergoes in the crystal. As an example, for 60-keV Si ions, the TRIM Monte-Carlo code[10] calculates that after penetrating 10 nm of GaAs, the distribution of ion angles is Gaussian (as in most theories of multiple scattering[24]) with a width $\sigma_\theta = 20°$. Therefore, although one may use angles that directly avoid impinging on a channel, scattering into any number of axial or planar channels is possible after the ion enters the crystal. For high-index planar and axial channels, the ion lifetimes in the channel are short. Nevertheless, this type of channeling will contribute to the channeling tails. Therefore, independent of the initial tilt and rotation angles chosen for the implant, there will doubtless be some minimum channeling tail.

We made a series of measurements at different tilt and rotation angles. A simple goniometer was constructed for our implantor that allowed samples, cleaved parallel to the wafer flat, to be implanted at precisely selected tilt and rotation angles. The uncertainties in these angles are approximately ±1°. Samples were also implanted in a standard implantor at a tilt angle of 7°. Here the different rotation angles were obtained by bonding the samples to 4-in. Si wafers at the desired rotation angles, allowing the simultaneous implantation of six different rotation angles. The relative uncertainties in these rotation angles are less than 1.5° (resulting from the accuracy of the bonding and the beam scan

Downloaded 08 Aug 2003 to 128.112.49.65. Redistribution subject to AIP license or copyright, see http://ojps.aip.org/japo/japcr.jsp

angle over the limited part of the Si wafer where the samples were placed). The absolute uncertainty is about 2.5°, due to the placement of the Si wafer in the implantor.

Figure 8 shows SIMS results obtained for 60-keV Si for selected tilt angles, with a constant rotation angle of 10°. Narrower profiles are obtained at large tilt angles for two reasons: the reduction of ion channeling and the simple projection of the distributions onto the depth direction, according to cos θ_{tilt}. For the small tilt angles shown in Fig. 8, the projection narrows the profiles by only 0.98, which is clearly a negligible effect compared to the observed narrowing between 2° and 11°. The broader width of the profiles at low angles is due to a combination of axial and planar channeling. One cannot completely avoid the channeling tails; for $\theta > 10°$, the profiles are nearly independent of the tilt angle (aside from the projection effect), but do not approach the Gaussian, predicted for implantation into amorphous material. Similar results were obtained for 100- and 240-keV Si ion implantation into GaAs,[1,5] and for implantation of various ions into Si wafers.[4,6-8]

In Fig. 9, we plot the rotation-angle dependence for 20-keV Be implantation into GaAs, for a tilt angle of 7°. Since in this case $2\psi_c$ is $\sim 11°$, channeling into the (011) plane cannot be avoided for any rotation angle at this tilt, although slightly narrower profiles can be obtained at large rotation angles, as is clearly seen in the figure.

For 200-keV Be ion implantation, $2\psi_c$ is 3°. With $\theta_{tilt} = 7°$, θ_{110} is greater than $2\psi_c$ for rotation angles greater than 10°, significantly reducing (011) planar channeling. As is seen in Fig. 10, the profile for 0° rotation is much broader than those obtained for all other angles, in agreement with this expectation. In several cases, we purposely implanted at rotation angles to enhance channeling into minor planes mapped by Ziegler and Lever.[3] Aside from the (011), the most significant should be the (400) at a rotation angle of 45°. However, impinging on these minor planes is seen to have no measurable effect on the channeling tails; identical profiles are seen at nearby rotation angles.

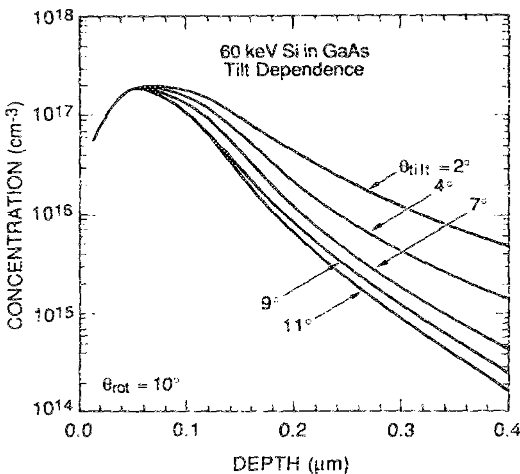

FIG. 8. Measured concentration profiles for 60-keV Si ions implanted into bare GaAs wafers at tilt angles from 2° to 11°, for a constant rotation angle of 10° (except: $\theta_{rot} = 26°$ for $\theta_{tilt} = 11°$). The measured profiles are smoothed for clarity.

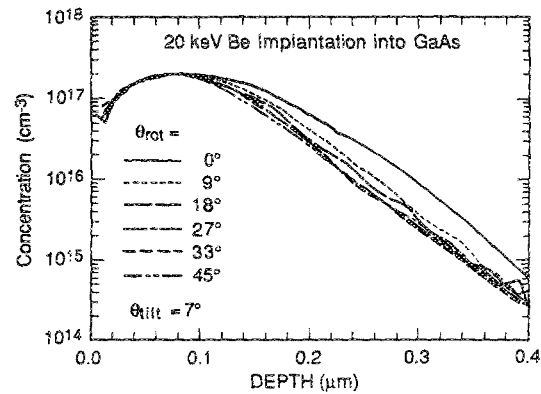

FIG. 9. Measured concentration profiles for 20-keV Be ions implanted into GaAs for selected rotation angles from 0° to 45°, for a constant tilt angle of 7°.

By implanting through amorphous overlayers, a reduction in the dependence of the implant profiles on the tilt and rotation angles can be achieved.[1] The overlayer scatters the beam sufficiently to reduce the fraction of ions directly impinging upon the axial or planar channels. For example, the difference between the profiles resulting from the $\theta_{rot} = 0°$ implant and other rotation angles for 200-keV Be ions implanted through a 45-nm cap Si_3N_4 layer is smaller than that seen for the bare-wafer implants (Fig. 10).

C. Dose dependence

Due to the lattice displacements produced by the stopping of heavy ions in crystalline GaAs, one can expect to heavily damage the crystal in the region where the ion comes to rest. At high doses, a profile that is closer to Gaussian or Pearson-I profiles, predicted by the amorphous implant

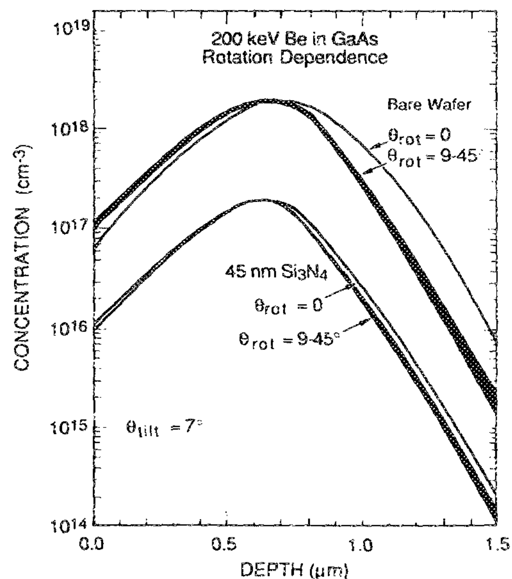

FIG. 10. Measured concentration profiles for 200-keV Be ions implanted into bare and capped (45-nm Si_3N_4) GaAs wafers for selected rotation angles from 0° to 45° and at a constant tilt angle of 7°. The wide black lines indicate the envelope of the data obtained for five rotation angles between 9° and 45°.

Downloaded 08 Aug 2003 to 128.112.49.65. Redistribution subject to AIP license or copyright, see http://ojps.aip.org/japo/japcr.jsp

codes, should then be obtained.[10] On the other hand, high implant ion currents can cause the wafer temperatures to rise, resulting in some self-annealing taking place, thus repairing the damage, and resulting in the same relative channeling tails being obtained for both low and high doses. In some Si device fabrication processes, the crystal is purposely heavily damaged to suppress channeling. Producing heavy damage in GaAs is not desirable, since residual defects usually remain following the post-implant anneal, resulting in electrically active traps, low ion activation, and poor electron mobilities.

To be of use for the fabrication of MESFET devices, the profiles calculated with our analytical formulas should be valid for doses between 10^{12} and 10^{13} ions/cm^2, typically used for the MESFET active channel. Doses higher than 10^{13} cm^{-2} are sometimes used to implant the source and drain contact regions of MESFETs, but device characteristics are not critically dependent on the shape of those profiles. To assure that the profiles are independent of ion dose below the 10^{13} dose we used for most of our work, implants of 3×10^{12} to 10^{15} ions/cm^2 were done. Figure 11 shows profiles for 100-keV Si ions, normalized to same peak concentration. At higher doses, narrower profiles are observed. Yeo *et al.*[25] obtained similar results for 120-keV Mg ions in GaAs, and we obtained similar results for 40- and 200-keV Be and 25-, 60-, and 200-keV Si ion implants. The reduction of the channeling tails is smaller for Be than for the more heavily damaging Si ions. Consistent results are obtained below 10^{13} ions/cm^2, so that the results given in Sec. III A for profiles measured for 10^{13} ions/cm^2 doses should be valid for implant doses of 10^{12} cm^{-2}.

Selenium produces the most damage, and Se ion implantation showed the greatest effect of increasing dose on the profiles, as seen in Fig. 12. Between 10^{13} and 5×10^{13} ions/cm^2, the magnitudes of the channeling tails decreased, with the reduction beginning to saturate above 10^{14} cm^{-2}. Despite the very high doses and resultant damage, we never obtained profiles close to those for implantation into amorphous GaAs.[10] This may be due to self-annealing effects associated with wafer heating for the high doses. (In the high-current Se implants, the wafer temperatures became sufficiently high to partially melt the photoresist used to bond the samples onto Si wafers.)

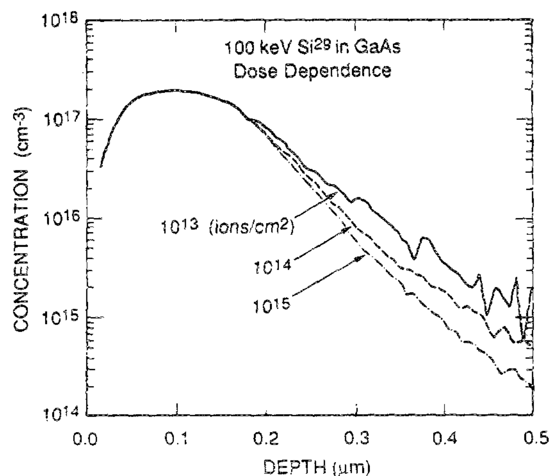

FIG. 11. Measured concentration profiles for 100-keV ^{29}Si ions implanted into bare GaAs wafers at doses of 10^{13}, 10^{14}, and 10^{15} ions/cm^2. The profiles have been normalized to the same peak height, 2×10^{17} cm^{-3}.

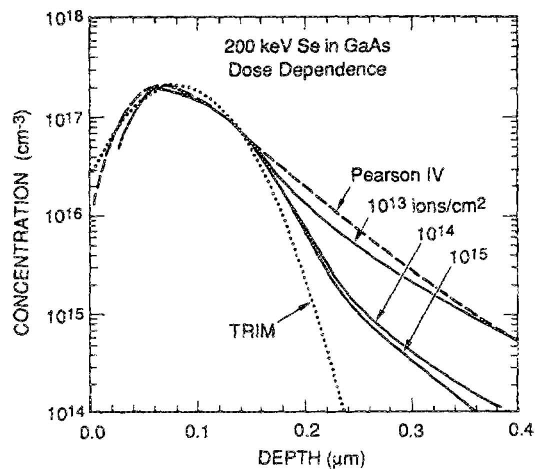

FIG. 12. Normalized, measured concentration profiles for 200-keV Se ions implanted into bare GaAs wafers at doses of 10^{13}, 10^{14}, and 10^{15} ions/cm^2. Fitted Pearson-IV profiles, and a TRIM (Ref. 10) calculated profile for implantation into amorphous GaAs are shown for comparison.

Figure 12 suggests that to obtain narrower profiles, a room-temperature damage implant with As (being similar to Se) at 5×10^{13} ion/cm^2 is sufficient. The additional damage may result in high post-implant trap concentrations,[26] though there is some evidence that using As ions may result in increased activation for subsequent Si implants.[27]

D. Dislocation density dependence

The commercial, high-pressure–grown GaAs wafers used in our studies have typical dislocation densities of $(3–8)\times10^4$ cm^{-2}.[28] In a typical SIMS measurement, the sputter crater diameter is about 100 μm, so approximately six dislocations are expected to be present in every measurement. To investigate whether these dislocations might scatter the implant-ion beam sufficiently to affect the channeling tails,[29] we compared profiles for low-dislocation, In-doped wafers and conventional wafers,[30] both implanted with 10^{13} 60-keV Si, 200-keV Se, and 100-keV Be ions/cm^2. For the (2%) In-doped wafers, varying dislocation densities are obtained in the middle of the wafer (3000 cm^{-2}), in a ring approximately 1 in. in diameter on a 3-in. wafer (500 cm^{-2}), and on the outer part of the wafer (800 cm^{-2}). We also compared conventional wafers having a dislocation density equal to 45 000 cm^{-2}. As seen in Fig. 13, identical implant profiles are obtained with all dislocation densities for Se. Similar results are obtained for Si and Be implantation.

We conclude that the results obtained in Sec. III A for implantation into high-dislocation material should also be valid for implantation into low-dislocation, In-doped material.

E. Implantation through caps

In the fabrication of GaAs devices, implantation through 40- to 100-nm Si_3N_4 or SiO_2 encapsulants is some-

Downloaded 08 Aug 2003 to 128.112.49.65. Redistribution subject to AIP license or copyright, see http://ojps.aip.org/japo/japcr.jsp

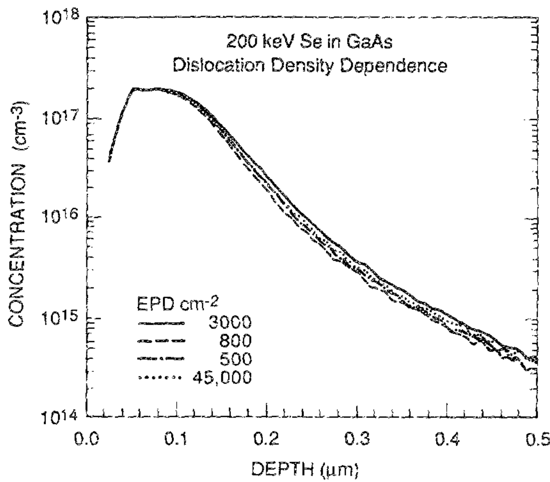

FIG. 13. Measured concentration profiles for 200-keV Se ions implanted into bare GaAs wafers with selected dislocation densities, obtained by using In-doped GaAs wafers (etch-pit density = 500, 800, and 3000 cm^{-2}) and conventional wafers (EPD = 45 000 cm^{-2}).

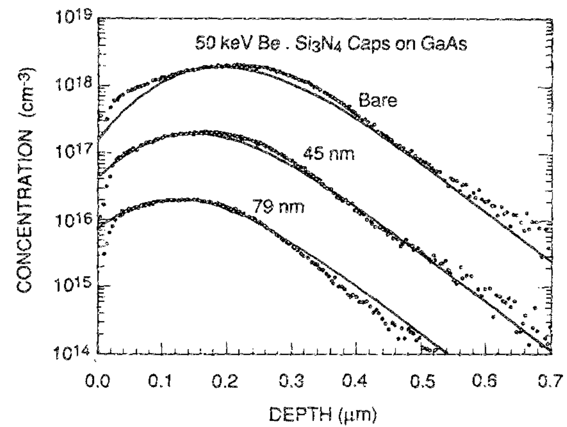

FIG. 14. Measured concentration profiles for 50-keV Be implanted into bare GaAs wafers and wafers with 45- and 79-nm CVD Si_3N_4 caps, compared with fits using the range-scaling theory, Eq. (8).

times done. These caps prevent the decomposition of GaAs during subsequent post-implant annealing, and also prevent the deposition of contaminants onto the surface and possible surface decomposition resulting from wafer heating during the implant and other processing. We have seen in Sec. III B that implanting through caps reduces the dependence of the channeling tails on the wafer rotation angle, a variable not often accurately controlled in many manufacturing facilities.

We have measured the profiles for Si, Se, and Be ions in GaAs, implanted through 40–200-nm plasma-enhanced chemical-vapor-deposition (PECVD) Si_3N_4 and CVD SiO_2 layers. The estimated cap densities are 2.9 and 2.2 g/cm^3, respectively.

For Be ions, implanting through caps mainly just shifts the origin of the implant profiles. The range scaling theory[20-22] was developed to describe the concentration distributions both in the cap $C_{\rm cap}(x)$ and the semiconductor C_s. Since the caps are amorphous, TRIM[10] or other amorphous profile simulators can be used to calculate those concentration distributions. In the underlying semiconductor, the concentration is given by

$$C(x) = C_s(x - t_{\rm cap} R_{ps}/R_{p{\rm cap}}), \tag{8}$$

where x is measured from the surface of the semiconductor, and R_{ps} and $R_{p{\rm cap}}$ are the projected ranges of the ions in the semiconductor and in the encapsulant, respectively. In the present case, we use the Pearson-IV profiles, derived for implantation into unencapsulated wafers in Sec. III A, to estimate C_s. The amorphous implants are usually described analytically by Gaussians (Si and Se ions) or by Pearson-I profiles (Be ions). The ion dose lost in the cap is obtained by integrating over the profile in the cap:

$$\Phi_{\rm cap} = \int_0^{t_{\rm cap}} dx'\, C_{\rm cap}(x'), \tag{9}$$

and the concentration in the GaAs is then normalized to the total implant dose Φ minus $\Phi_{\rm cap}$.

For the ion range in the semiconductor, R_{ps}, a choice must be made whether to use the amorphous range, consistent with $R_{p{\rm cap}}$, or the larger, experimentally determined projected range shown in Fig. 2, which is influenced by channeling. In fitting the measured profiles of Be ions implanted through caps, we find that using the amorphous range gives better agreement with the data, as shown in Fig. 14. Similar results are obtained for 100–400 keV Be^+ ion implants through 50–200-nm Si_3N_4 and SiO_2 caps.

We have also calculated the amorphous ranges, and the longitudinal and lateral straggling parameters using the TRIM Monte-Carlo code.[10] In this calculation, about 2000–5000 ion trajectories are followed, and the ranges are fit to power-law functions of the ion energy, e.g.,

$$R_{pi} = AE^B. \tag{10}$$

The parameters A and B determined for implantation into GaAs, Si_3N_4, and SiO_2 are listed in Table I. For caps with different densities, one scales the three moments inversely with density. For the densities listed, we generally find that the ratio of R_p values in Eq. (8) is near unity for Si_3N_4 and about 2/3 for SiO_2 encapsulants.

TABLE I. Amorphous ranges R_p, straggling ΔR_p, and lateral straggling ΔR_l. Power-law parameters [Eq. (10)][a].

Ion	Substrate[b]	R_p		ΔR_p		ΔR_l	
		A	B	A	B	A	B
Si^{29}	GaAs	13.021	0.951	13.461	0.777	11.477	0.831
Si	Si_3N_4	11.187	0.983	9.223	0.773	5.371	0.870
Si	SiO_2	13.850	1.020	12.349	0.793	6.341	0.919
Se^{80}	GaAs	6.049	0.932	4.698	0.830	3.423	0.860
Se	Si_3N_4	7.853	0.902	3.211	0.836	2.319	0.839
Se	SiO_2	11.499	0.892	4.893	0.813	3.536	0.822
Mg^{24}	GaAs	15.770	0.952	15.898	0.781	13.095	0.851
Mg	Si_3N_4	13.532	0.986	13.175	0.732	6.596	0.881
Mg	SiO_2	17.901	1.002	15.381	0.779	8.765	0.903
Be^9	GaAs	54.931	0.846	47.144	0.647	55.350	0.694
Be	Si_3N_4	47.828	0.882	39.607	0.583	28.388	0.724
Be	SiO_2	69.352	0.882	60.177	0.576	56.138	0.585

[a] The moments are in Å, when the ion energy is in keV.
[b] Densities: GaAs: 5.32 g/cm^3; Si_3N_4: 3 g/cm^3; SiO_2: 2.2 g/cm^3.

Downloaded 08 Aug 2003 to 128.112.49.65. Redistribution subject to AIP license or copyright, see http://ojps.aip.org/japo/japcr.jsp

The magnitudes of the channeling tails are reduced when Si and Se ions are implanted through caps. This is illustrated in Fig. 15, together with the method used to fit this reduction. For 100-keV Si implants through 79-nm Si_3N_4 caps, simply shifting the Pearson-IV profile, obtained for implants into bare wafers, results in a larger magnitude of the tail at large depths, though it accurately predicts the shape of the measured distributions at large depths. We fit the measured distribution by reducing the magnitude of the shifted Pearson-IV [calculated using Eq. (8)], by a factor of 0.25. For the remaining part of the distribution, a shifted Gaussian, calculated using the TRIM parameters in Table I, and Eq. (8) is used to describe the shift. Both the Pearson-IV and Gaussian distributions are normalized to unity at $x = R_p$, so the mixture can be described by a single parameter f

$$C(x) = (1-f)C_{s\mathrm{Gaus}}(x) + fC_{s\mathrm{PIV}}(x). \qquad (11)$$

The net concentration is then normalized to the integrated dose or to an arbitrary peak height, as shown in Fig. 15.

Presently, insufficient data exist to obtain a universal parametrization for the parameter f. Probably, f depends on the ratio of the cap thickness to R_p in the semiconductor. Fits for other 100-keV Si ion implants are shown in Fig. 16. The Pearson-IV fraction is seen to decrease as the cap thickness increases. Apparently, for the relatively deeper Be ion implants, the cap thickness is not sufficiently large compared to R_p to observe a reduction in f. Also, electronic stopping dominates the Be energy loss in the caps, so the Be ions are not scattered as much as the Si and Se ions. As more data become available for Si and Se implantation, further parametrization of this effect will be done.

F. Knock-on distributions

When one implants into GaAs through Si_3N_4 or SiO_2 caps, Si and N or O atoms are knocked forward by the implant ion into the GaAs.[11,31] The "knock-on" Si recoils in the GaAs are additional donors, which add to the effective concentration of donors in the GaAs, while the O recoils can either form deep-donor traps or can compensate the implanted donors.

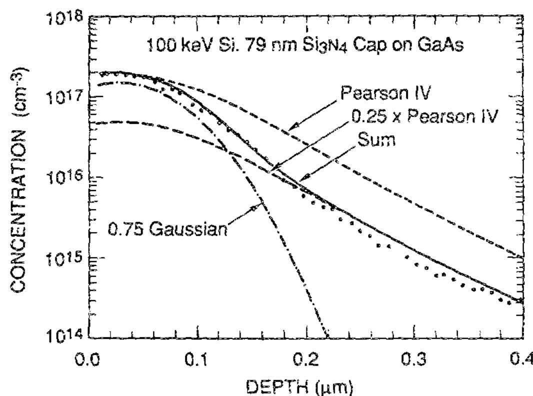

FIG. 15. Measured concentration profiles for 100-keV Si implanted into GaAs through 79-nm CVD Si_3N_4 caps, compared with calculated fits.

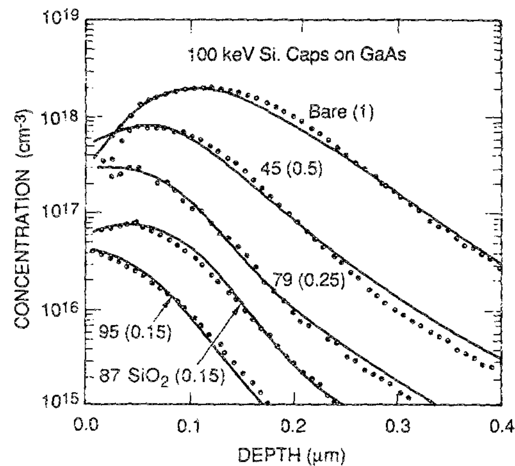

FIG. 16. Measured concentration profiles for 100-keV Si implanted through PECVD Si_3N_4 and one CVD SiO_2 cap into GaAs. The numbers give the cap thickness in nm, and the numbers in parentheses give the Pearson-IV mixing factor f defined in Eq. (11).

It is difficult to measure the knock-on distributions, except for high implant doses. In the SIMS analysis of GaAs substrates, masses associated with O, N, and Si^{28} typically have large backgrounds. (Mass 28 is probably due to CO molecules.) We have measured knock-on distributions for an implant dose of 2×10^{15} 200-keV Se ions/cm^2 implanted through 87-nm SiO_2 caps. This dose is sufficiently high so we can measure knock-on Si^{29} from caps having the normal 4.7% Si^{29} abundance. The O knock-on distribution was measured by taking the difference between the O found after implanting through a SiO_2 cap and the O background found after implanting through a 74-nm sputtered Si_3N_4 cap. Similar Si knock-on distributions were observed for implants through the Si_3N_4 cap, but N atom concentrations could not be measured.

Figure 17 compares the measured knock-on distributions with TRIM calculations. As usual, the Se ion distribution has a large channeling tail, though it is not as large for these high dose implants, as it would be for a low-dose one

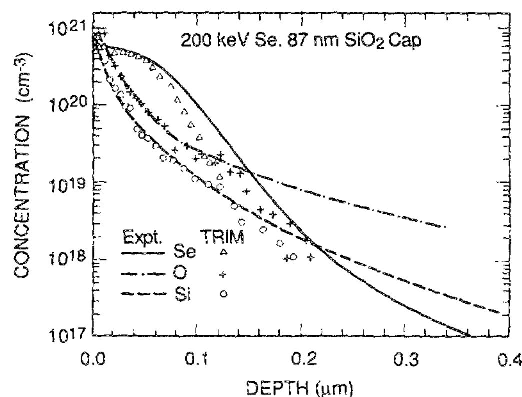

FIG. 17. Measured (lines) and TRIM calculations (points) of the concentration profiles of Se ions, and recoiled Si and O atoms, after implantation of 2×10^{15} 200-keV Se ions/cm^2 through an 87-nm SiO_2 cap on GaAs.

Downloaded 08 Aug 2003 to 128.112.49.65. Redistribution subject to AIP license or copyright, see http://ojps.aip.org/japo/japcr.jsp

(Fig. 12). The magnitudes of the Si and O knock-on concentrations agree roughly with the TRIM calculations for shallow depths, but like the Se ion implants, they exhibit longer tails than predicted by TRIM.

Since the recoil concentrations are largest at the surface where channeling tails are still not significant, we conclude that TRIM profiles may be adequate for simulating recoil-atom profiles for MESFET process and device modeling.

G. Electron profiles

In much earlier work on ion implantation into GaAs, comparisons were made between measured electron carrier profiles and ion profiles, calculated using the LSS theory.[32] When diffusion effects during the post-implant activation anneals were negligible, generally reasonable, qualitative agreement was found between the LSS Gaussian profiles and the electron profiles, with the exponential channeling tails either not being observed, or being much smaller than what we have observed in the atomic profiles.

It should be noted that ion implantation into semi-insulating LEC GaAs is comparable to implantation into p^- substrates.[33] The intersection between the implanted shallow donor and the background shallow acceptor profiles [typically $N_A = (1\text{–}6\times10^{15}\ \text{cm}^{-3}$ C or $> 10^{16}\ \text{cm}^{-3}$ Cr] forms a substrate junction, with a corresponding depletion region extending toward shallow depths. This depletion region acts to cut off the tails of the implanted donor distributions, resulting in measured, near-Gaussian electron profiles.

We illustrate this in Fig. 18, where measured donor and carrier profiles are compared with a calculated electron profile, obtained by solving Poisson's equation for zero bias at the surface. The implants used were 5×10^{12} 100-keV Si^{29} ions/cm^2, at $\theta_{\text{tilt}} = 8°$ and $\theta_{\text{rot}} = 10°$ into lightly Cr-doped LEC GaAs. The implant was activated using an 850 °C, 15-min capless anneal in an As overpressure, giving an activation of $\sim 80\%$. We measured the Cr profiles in the annealed wafers and found them to be about $3\times10^{15}\ \text{cm}^{-3}$ in the bulk and about $1\times10^{15}\ \text{cm}^{-3}$ at the surface, due to Cr out-diffusion, with a typical fall-off length of about 1 μm. We assume no Si diffusion during this anneal.[34] The calculated electron profile is clearly in good agreement with the electron profile measured using the capacitance-voltage (C-V) method down to concentrations of $\sim 10^{16}\ \text{cm}^{-3}$.

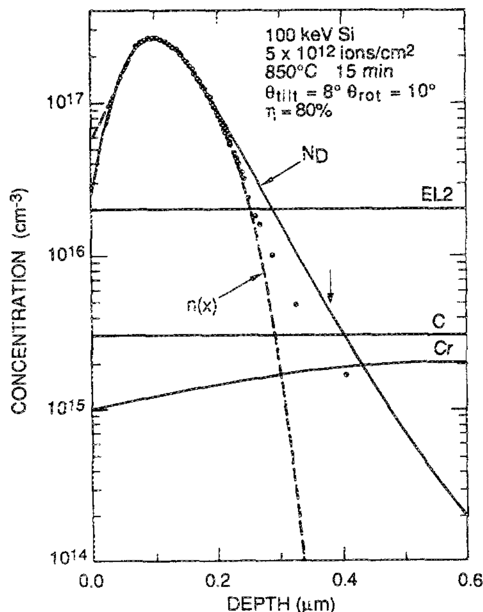

FIG. 18. Comparison of measured Si^{29} donor profiles (solid line), resulting calculated electron profiles [solutions to Poisson's equation for $n(x)$ with zero bias; dashed line], and measured electron profiles, determined using the C-V method (points). Also shown are the EL2, C, and Cr concentrations assumed or measured in the calculations of $n(x)$.

Beyond this point, tails are observed in the C-V-measured electron profiles. The tails can occur as a result of series resistance in the capacitance measurement when the resistance of the depleted region becomes significant. Corrections for this effect can be made by monitoring the phase angle during the rf measurement or by making RC corrections to the capacitance.[35] The latter has been done for the C-V profiles shown in Fig. 18. However, a more fundamental limitation of the C-V method at these concentrations is that the width of the carrier profile under reverse bias becomes comparable to the Debye length, so that the approximations upon which the C-V measurement of $n(x)$ depends break down. Care should be taken before attempting to relate tails on C-V-measured carrier profiles to tails in the atomic-impurity profiles.

For process and device modeling, it is important to begin with the correct implant profiles. Although one can apparently use LSS or near-Gaussian profiles to qualitatively predict electron profiles up to where the C-V profiles break down, one should not use LSS profiles instead of atomic-impurity profiles since the substrate junction will further narrow the LSS profiles, giving unrealistic device characteristics, as will be illustrated in a subsequent paper.

IV. CONCLUSIONS

Profiles measured for Be, Si, and Se implantation into unencapsulated GaAs wafers at energies between 20 and 400 keV have been fit to Pearson-IV distributions, and the resulting fitting parameters were fit to functions of the ion energy to derive simple, analytical formulas for implant profiles for any energy between about 10 and 400 keV.

Profile measurements for selected wafer tilt and rotation angles show that the narrowest profiles for a given ion energy occur for tilt angles greater than 7° and rotation angles of 45°. Implantation through wafers encapsulated with Si_3N_4 or SiO_2 layers reduces the dependence of the profiles on the rotation angle.

The profiles are not dependent on the wafer dislocation density for densities between 500 and 50 000 cm^{-2}, nor on In doping of the wafers.

Channeling tails on the profiles can be reduced slightly for Si and Be ions by using high ion doses of either the bombarding ion or a similar, but electrically inactive, damage-producing ion. Se ions have the greatest effect on reducing channeling tails, although it is unclear whether the possibly beneficial effect of reducing tails might be outweighed by

Downloaded 08 Aug 2003 to 128.112.49.65. Redistribution subject to AIP license or copyright, see http://ojps.aip.org/japo/japcr.jsp

undesirable effects of trap formation, low ion activation, and poor electron mobilities.

For Be implants through SiO_2 and Si_3N_4 encapsulants on GaAs, the profiles in the GaAs can be predicted by simply shifting the profile for implantation into unencapsulated wafers by an amount related to the cap thickness. For Si and Se, our measurements suggest that the channeling tails are reduced slightly by implanting through caps. We presently have insufficient data to derive a universal function describing this reduction. The distributions of Si knock-on ions after implantation through caps are predicted accurately using TRIM Monte-Carlo calculations at shallow depths.

The results presented in this work have been incorporated into two process and device models, SUPREM 3.5 (Ref. 36) and GATES.[37] SUPREM 3.5 is a general process model, designed to work in conjunction with Stanford University's one- and two-dimensional device simulators, SEDAN and PISCES. GATES, standing for gallium arsenide transistor engineering models, is a combined process and device modeling program for GaAs MESFET technology. These models are both available to the GaAs integrated-circuit industry.[38]

ACKNOWLEDGMENTS

This work would not have been possible without the support of both the Wright-Patterson Air Force Materials Laboratory [Contract No. F33615-85-C-5048 (W. Mitchel)] and the Defense Advanced Research Projects Agency [Contract No. DAAL-01-86-K-0101]. Also, we thank many analysts at Charles Evans and Associates for SIMS analysis, IICO Implant Services, CRAY Research for making some of the earlier implants for us, D. Holmes at Rockwell International for providing In-doped wafers, Ron Besser of Watkins-Johnson for depositing PECVD Si_3N_4 caps, and the Rockwell Microelectronics GaAs pilot line for depositing the SiO_2 caps. This work has also benefited from private communications with J. P. Biersack, M. Giles, and D. Rosenblatt. The *C-V* data, shown in Fig. 18, were measured by D. Rosenblatt at Watkins-Johnson.

[1] R. T. Blunt and P. Davies, J. Appl. Phys. **60**, 1015 (1986).
[2] J. Kasahara, H. Sakurai, T. Suzuki, M. Arai, and N. Watanabe, *Technical Digest, 1985 GaAs IC Symposium* (IEEE, Piscataway, NJ, 1985), p. 37.
[3] J. F. Ziegler and R. F. Lever, Appl. Phys. Lett. **46**, 358 (1985).
[4] K. Cho, W. R. Allen, T. G. Finstad, W. K. Chu, G. J. Liu, and J. J. Wortman, Nucl. Instrum. Methods B **7/8**, 265 (1985).
[5] D. Rosenblatt, W. R. Hitchens, R. Anholt, and T. W. Sigmon, IEEE Electron Device Lett. **EDL-9**, 139 (1988).
[6] M. I. Current, N. L. Turner, T. C. Smith, and D. Crane, Nucl. Instrum. Methods B **6**, 336 (1985).
[7] R. B. Liebert, D. F. Downey, and V. K. Bason, Nucl. Instrum. Methods B **21**, 391 (1987).
[8] A. E. Mitchel, R. H. Kasel, S. R. Mader, B. J. Masters, and J. A. Gardner, Appl. Phys. Lett. **44**, 404 (1984).
[9] J. F. Gibbons, W. S. Johnson, and S. W. Mylroie, *Projected Range Statistics* (Dowden, Hutchinson, and Ross, Stroudsburg, PA, 1975).
[10] J. P. Biersack and L. G. Haggmark, Nucl. Instrum. Methods **174**, 257 (1980).
[11] L. A. Cristel, J. F. Gibbons, and S. Mylroie, J. Appl. Phys. **51**, 6176 (1980).
[12] J. P. Biersack and J. F. Ziegler, *Ion Implantation Techniques* (Springer, New York, 1982), p. 122.
[13] J. F. Ziegler, J. P. Biersack, and U. Littmark, *The Stopping and Range of Ions in Solids* (Pergamon, New York, 1985), Vol. I.
[14] S. Sze, *Physics of Semiconductor Devices* (Wiley, New York, 1981), Chap. 6.
[15] M. T. Robinson and O. E. Oen, Phys. Rev. **132**, 2385 (1963).
[16] O. S. Oen and M. T. Robinson, Nucl. Instrum. Methods **132**, 647 (1976).
[17] M. T. Robinson, in *Sputtering by Particle Bombardment I*, edited by R. Behrisch (Springer, New York, 1981), Chap. 3.
[18] M. Giles, IEEE Trans. Computer Aided Design **CAD-5**, 679 (1986).
[19] T. Takeda, S. Tazawa, and A. Yoshii, IEEE Trans. Electron Devices **ED-33**, 1278 (1986).
[20] H. Ryssel and I. Ruge, *Ion Implantation* (Wiley, New York, 1986).
[21] S. Selberherr, *Analysis and Simulation of Semiconductor Devices* (Springer, Wien, 1984), Chap. 3.
[22] H. Ryssel and J. P. Biersack, in *Process and Device Modeling*, edited by W. L. Engl (North-Holland, Amsterdam, 1986).
[23] Formulas for Pearson-IV distributions can be found in Refs. 20–22. To avoid computer overflow errors, calculate the log of the distribution, and subtract the log of the distribution at $x = R_p$ before taking the exponential, and normalizing the resulting distribution to the ion dose.
[24] J. D. Jackson, *Classical Electrodynamics* (Wiley, New York, 1962), Chap. 13.
[25] Y. K. Yeo, Y. S. Park, F. L. Pedrotti, and B. D. Choe, J. Appl. Phys. **53**, 6148 (1982).
[26] D. W. E. Allsopp and A. R. Peaker, Solid-State Electron. **29**, 467 (1986).
[27] A. R. von Neida, S. J. Pearton, M. Stavola, and R. Carusso, Appl. Phys. Lett. **49**, 1708 (1986).
[28] Boule data sheet, Dow Chemical Co.
[29] W. A. Coghlan, M. N. Rhee, J. M. Williams, L. A. Streit, and P. Williams, Nucl. Instrum. Methods B **16**, 171 (1986).
[30] The In-doped wafers were grown by D. Holmes and co-workers at Rockwell International.
[31] M. J. Tejwani and P. Riemenschneider, Nucl. Instrum. Methods B **21**, 471 (1987).
[32] D. V. Morgan, F. Eisen, and A. Ezis, IEE Proc. Pt. I **128**, 109 (1981).
[33] R. Anholt and T. W. Sigmon, J. Appl. Phys. **62**, 3995 (1987).
[34] H. Kanber, M. Feng, V. K. Eu, R. C. Rush, and W. B. Henderson, J. Electron. Mater. **11**, 1083 (1982).
[35] R. E. Williams, *GaAs Processing Techniques* (ARTECH, Dedham, MA, 1984), p. 368.
[36] M. D. Deal, S. E. Hansen, R. Anholt, S. Chou, J. D. Plummer, R. W. Dutton, T. W. Sigmon, D. A. Stevenson, C. R. Helms, and J. C. Bravman, *Proceedings of the 1987 IEEE IEDM Conference* (IEEE, Piscataway, NJ, 1987), p. 245.
[37] R. Anholt, T. W. Sigmon, and M. Deal, *Technical Digest, 1987 GaAs IEEE IC Symposium* (IEEE, Piscataway, NJ, 1987), p. 51. (GATES was called GEM in this paper).
[38] Contact M. D. Deal, Center for Integrated Systems, Stanford University concerning SUPREM 3.5; R. Anholt, Gateway Modeling (612-339-4239) for GATES.

Downloaded 08 Aug 2003 to 128.112.49.65. Redistribution subject to AIP license or copyright, see http://ojps.aip.org/japo/japcr.jsp